Viral dynamic modeling of SARS-CoV-2 in non-human primates

Antonio Gonçalves (antonio.goncalves@inserm.fr)
Université de Paris / INSERM https://orcid.org/0000-0002-8759-2429

Pauline Maisonnasse
CEA - Université Paris Saclay - INSERM U1184 https://orcid.org/0000-0002-0555-207X

Flora Donati
Unité de Génétique Moléculaire des Virus à ARN, GMVR : Institut Pasteur, UMR CNRS 3569
https://orcid.org/0000-0003-2862-9751

Mélanie Albert
Unité de Génétique Moléculaire des Virus à ARN, GMVR : Institut Pasteur, UMR CNRS 3569
https://orcid.org/0000-0002-3826-8729

Sylvie Behillil
Unité de Génétique Moléculaire des Virus à ARN, GMVR : Institut Pasteur, UMR CNRS 3569

Vanessa Contreras
Université Paris-Saclay, Inserm, CEA, Center for Immunology of Viral, Auto-immune, Hematological and Bacterial diseases

Thibaut Naninck
CEA – Université Paris Saclay – INSERM U1184

Romain Marlin
CEA

Caroline Solas
Aix-Marseille University

Andres Pizzorno
CIRI, Centre International de Recherche en Infectiologie, (Team VirPath), Univ Lyon

Julien Lemaitre
Université Paris-Saclay, Inserm, CEA, Center for Immunology of Viral, Auto-immune, Hematological and Bacterial diseases

Nidhal Kahlaoui
Université Paris-Saclay, Inserm, CEA, Center for Immunology of Viral, Auto-immune, Hematological and Bacterial diseases

Olivier Terrier
CIRI, Centre International de Recherche en Infectiologie, (Team VirPath), Univ Lyon, Inserm, U1111, Université Claude Bernard Lyon 1, CNRS, UMR5308, ENS de Lyon https://orcid.org/0000-0001-9393-7684

Raphael Ho Tsong Fang
Université Paris-Saclay, Inserm, CEA, Center for Immunology of Viral, Auto-immune, Hematological and Bacterial diseases
Vincent Enouf
Institut Pasteur
Nathalie Dereuddre-Bosquet
CEA https://orcid.org/0000-0001-6682-6313
Angela Brisbarre
Unité de Génétique Moléculaire des Virus à ARN, GMVR : Institut Pasteur, UMR CNRS 3569
Franck Touret
UVE Aix Marseille Univ, IRD 190, INSERM 1207, IHU Méditerranée Infection https://orcid.org/0000-0002-4734-2249
Catherine Chapon
CEA, Division of Immuno-Virology, Institute for Emerging Diseases and Innovative Therapies (iMETI)
Bruno Hoen
Emerging Diseases Epidemiology Unit, Institut Pasteur
Bruno Lina
CIRI, Centre International de Recherche en Infectiologie, (Team VirPath), Univ Lyon, Inserm, U1111
Manuel Rosa-Calatrava
Université Lyon 1
Xavier de Lamballerie
Aix Marseille Univ https://orcid.org/0000-0001-7895-2720
France Mentré
French Institute of Health and Medical Research
Roger Le Grand
Université Paris-Saclay, INSERM, CEA https://orcid.org/0000-0002-4928-4484
Sylvie van der Werf
Institut Pasteur https://orcid.org/0000-0002-1148-4456
Jeremie Guedj
INSERM https://orcid.org/0000-0002-5534-5482

Article

Keywords: Viral dynamics, SARS-CoV-2, Hydroxychloroquine, non-human primates

Posted Date: August 4th, 2020

DOI: https://doi.org/10.21203/rs.3.rs-50301/v1

Abstract

Non-human primates infected with SARS-CoV-2 exhibit mild clinical signs. Here we used a mathematical model to characterize in detail the viral dynamics in 31 cynomolgus macaques infected with 10^6 pfu of SARS-CoV-2 for which nasopharyngeal and tracheal viral load were frequently assessed. We identified that infected cells had a large daily viral production (>10^4 virus) and a within-host reproductive basic number of 6 and 4 in nasopharyngeal and tracheal compartment, respectively. After peak viral load, infected cells were rapidly cleared with a half-life of 9 hours, with no significant association between cytokine elevation and clearance. Translating our model to the context of human-to-human infection, human mild infection may be characterized by a peak occurring 4 days after infection, a viral shedding of ~11 days and a generation time of 4 days. These results improve the understanding of SARS-CoV-2 viral replication and better understand the infection to SARS-CoV-2 in humans.

Introduction

The severe acute respiratory syndrome coronavirus 2 (SARS-CoV-2) which originated in Wuhan, China, at the end of December 2019, has spread rapidly around the world, resulting at the end of July 2020 in more than 500,000 deaths [1]. Fortunately, the majority of infections do not lead to hospitalizations, and about 80% of subjects infected with SARS-CoV-2 will experience asymptomatic or pauci-symptomatic infection characterized by specific (anosmia) or general symptoms (fever, fatigue) [1–3]. However, in 20% of cases evolution toward more severe symptoms can take place leading to pneumonia or acute respiratory distress syndrome [4]. In other acute or chronic viral diseases (HIV, HCV, influenza), the characterization of viral load kinetics has played an important role to understand the pathogenesis of the virus and design better antiviral drugs [5–7]. In the case of SARS-CoV-2, viral kinetics remain poorly characterized and its association with disease evolution is controversial. This is due to the fact that many studies rely on large transversal analyses with few patients having serial data points or, in contrary, on detailed small series of patients, often with mild diseases [8–10]. In that perspective, the analysis of data generated in non-human primates is a unique opportunity to characterize in detail the viral dynamics during natural infection, and to study the effects of antiviral therapy [11–13].

Here, we used data generated on nonhuman primates (NHP) infected by SARS-CoV-2. In this study, 31 cynomolgus macaques were infected with 10^6 pfu of a SARS-CoV-2 isolate and treated with hydroxychloroquine (HCQ) ± azithromycine (AZM) in either pre- or post-exposure prophylaxis [14]. Because our analysis did not find any support for any antiviral effect of HCQ against SARS-COV-2, we here analyzed together all animals and we neglected treatment with HCQ ± AZM as a first approximation. We develop a mathematical model of SARS-CoV-2 infection in NHP to provide estimation of key parameters driving viral dynamics.

Results

SARS-CoV-2 viral kinetics

A total of 31 animals were infected using a combined intra-nasal and intra-tracheal infection with 10^6 pfu of a primary SARS-CoV-2 isolate (BetaCoV/France/IDF/0372/2020). Animals developed a rapid infection, with viral loads peaking 2 days post infection (dpi) in both nasopharyngeal and tracheal compartments.After the peak, both nasopharyngeal and tracheal viral loads rapidly declined exponentially, with a median rate of 0.8 $\log_{10}$ copies/mL every day (**Fig. 1**).The slope in viral decline was more rapid in the trachea than in the nasopharynx, leading to a first measurement below the limit of quantification (LOQ=8514 copies/mL) 7 and 9 dpi, respectively. Overall, the area under the viral load curve (AUC) was larger in the nasopharynx than in the trachea (45 vs 38 $\log_{10}$ copies.day/mL, $p<10^{-4}$). Importantly, there was no evidence of an antiviral effect in animals receiving various doses of HCQ compared to those receiving vehicles, even after adjustement on HCQ exposure [14]. Thus, the effect of treatment was neglected as a first approximation. We later challenged this hypothesis but found no effect of HCQ in reducing viral production (see supplementary information file 1).

Viral kinetic model

Nasopharynx and trachea were considered as two distinct compartments of the upper respiratory tract (URT) where each one is described by a target cell limited model [11,15,16]. The model given by ordinary differential equations (1) to (5) describes theinterplay between susceptible cells (T), non-productive infected cell (I_1), productive cells (I_2) and infectious and non-infectious viruses (V^I and V^{NI}, respectively). The subscript X denotes the compartment of interest either nasopharynx or trachea. A schematic representation of the model is given in **Fig. 2**.

$$\frac{dT_X}{dt} = -\beta_X T_X V_X^I \quad (1)$$

$$\frac{dI_{1,X}}{dt} = \beta_X T_X V I_X - k I_{1,X} \quad (2)$$

$$\frac{dI_{2,X}}{dt} = k I_{1,X} - \delta_X I_{2,X} \quad (3)$$

$$\frac{dV_X^I}{dt} = p_X I_{2,X} \mu - c V_X^I \quad (4)$$

$$\frac{dV_X^{NI}}{dt} = p_X I_{2,X}(1-\mu) - c V_X^{NI} \quad (5)$$

Through respiration and movements of ciliary cells, viruses can migrate from one compartment to the other. Thus, we tested the possibility for viruses to exchange from nasopharyngeal to tracheal compartment and *vice versa* by linking both with a bidirectional rate constant *g*.However, due to the sparseness of the data, the parameter *g* could not be precisely estimated ($CI_{95\%}$ included 0) and was set to 0. Then, using a backward selection procedure we found that the infectivity rate β and the viral production *p* were different between nasopharyngeal and tracheal compartments (**Table 1**). For β, we found estimates of 1.8×10^{-4} and 2.5×10^{-5} mL/virion/day($p<10^{-4}$) and p was estimated to $1.9\times10^{4}$and 3.6×10^{4} virions/cell/day ($p<0.05$) in nasopharynx and trachea, respectively. However, viral production depends on the assumed initial number of target cells, T_0. For nasopharyngeal and tracheal

compartments, we assumed a total number of epithelial cells of 2.25×10^7 and 1.25×10^8 cells. Assuming that only 0.1% of cells express ACE2 receptors at their surface, we have 2.25×10^4 and 1.25×10^5 susceptible cells in nasopharynx and trachea, respectively. This leads to 4.4×10^8 and 4.5×10^9 virions/mL/day in nasopharynx and trachea respectively. The loss rate of infected cells, δ, was not found different between the two compartments and estimated to 1.88 d^{-1} corresponding to an infected cell half-life of 9 hours.

These parameter estimates allow us to derive the basic reproduction number R_0corresponding to the number of infected cells generated by a single infected cell at the beginning of the infection. We found $R_{0,N}$equal to 5.9 $(CI_{95\%} = [1.8 - 17.9])$ and $R_{0,T}$to 4.0 $(CI_{95\%} = [1.0 - 17.4])$. Together with the high inoculum in the trachea (see methods), the viral load scarcely increased in the trachea while clearly increased until 3 dpi in the nasopharynx (**Fig. 3**). One can also derive the viral burst size N corresponding to the number of viruses produced by an infected cell over its lifespan. We found N_N= 18,300 $(CI_{95\%} = [9{,}400 - 33{,}700])$ and N_T= 9,600 $(CI_{95\%} = [5{,}100 - 18{,}200])$.

Sensitivity analysis

Although values at which the viral clearance c and the eclipse rate k were fixed based on the current literature (10 d^{-1} and 3 d^{-1} respectively, see material and methods). We tested models with different values of these parameters. We considered 9 models resulting from the combination of models with c = 5; 10 or 20 d^{-1} and k = 1; 3 or 5 d^{-1}. Models assuming larger eclipse phase duration degraded the fit to the data with a substantial increase in the Bayesian Information Criterion (BIC) while other models were broadly undistinguishable from the reference model and within ~3 BIC points. Thus, we kept c = 10 d^{-1} and k = 3 d^{-1} for further analysis.

Immune markers during SARS-CoV-2 infection

Among the 30 cytokines tested, 6 greatly varied during the infection and peaked at 2 dpi, namely CCL11, CCL2, IFN-, IL-15, IL-1RA and IL-2 (**Fig. 4**). Spearman correlation tests were performed between the area under the cytokine curve and the predicted $\log_{10}$ AUC viral load, but there was no trends suggesting an association between cytokine and viral loads (**Fig. 5**).

We further considered potential association between IFN- and viral dynamics. For that purpose, we tested variations of models (Model 1 to 4, see supplementary information file 2) where IFN- levels over time, noted F(t), could modulate viral kinetic parameters. We considered 4 potential scenarios [11,15,16] where IFN could i) reduce infectivity by a factor 1/(1+φF(t)), ii) preserve φF(t) target cells from infection, iii) increase the loss of infected cells by a factor (1+φF(t)) and iv) lower viral production by a factor 1/(1+φF(t)). Overall, models assuming an increased infectivity or the formation of preserved cells showed a moderate gain in BIC (< 5 points) but did not provide better individual fits of the data. Thus, we did not consider those models for further analysis. Models, parameters estimates and individual fits of these models are provided in supplementary information file 2.

Simulation of a human infection

Given the physiopathology of a human infection by SARS-CoV-2, viral replication will start after the first cell is infected in both nasopharynx and trachea. By taking into account this aspect of the infection and scaling the compartments to human size (see methods), we predict that the viral load peak in human is 1.5×10^7 ($CI_{95\%} = [0.5 \times 10^7 - 3.2 \times 10^7]$) and 9.7×10^6 ($CI_{95\%} = [5.0 \times 10^6 - 18 \times 10^6]$) copies/mL in nasopharynx and trachea, respectively. In addition, the viral loads were predicted to be detectable during 10.4 ($CI_{95\%} = [8.9 - 16.6]$) and ($CI_{95\%} = 8.2\ [8.5 - 20]$) days in nasopharynx and trachea, respectively (**Fig. 6**). Lastly, we calculated the generation time T_g. Assuming that the infectiousness of the virus is proportional to the infectious viral loads, the generation time corresponds to the mean duration between infection of the index case and the subsequent infection of a contact. We found $T_{g,T}$= 2.4 ($CI_{95\%} = [1.8 - 3.8]$) days and $T_{g,N}$= 4.0 ($CI_{95\%} = [2.8 - 7.6]$) days suggesting that infectiousness was maximal within the first week of infection, but could still occur 2-3 weeks after infection.

Discussion

Based on a nonhuman primate (NHP) model of SARS-CoV-2 infection, we developed a mathematical model for SARS-CoV-2 that describes viral dynamics in both nasopharyngeal and tracheal swabs of 31 infected macaques. Using this model we could estimate key parameters of virus pathogenesis, in particular the production rate from infected cells (equal to 1.9×10^4 vs 3.6×10^4 virions/cell/day in tracheal and nasopharyngeal compartments, respectively), and the loss rate of infected cells, estimated to 1.88 d^{-1} in both compartments corresponding to a half-life of 9 hours. Consequently, we estimated the number of secondary cell infection resulting from one infected cells, R_0, to 4.0 and 5.9 cells in tracheal and nasopharyngeal compartments, respectively. This value of R_0, together with the large viral inoculum used in this experimental model (10^6 pfu), explains that tracheal viral loads barely increased post-infection and that nasopharyngeal viral loads rapidly peaked at 3 dpi. After peak viral load, the rapid loss rate of infected cells was sufficient to explain that clearance of the virus occurred around day 7 in both compartments, and we did not find evidence in this model for a role of an immune response mediated by cytokines in accelerating the viral clearance.

Although the number of animals and the very detailed kinetic data allowed a precise estimation of parameters, some hypotheses were made that will need to be confirmed. First, the estimation of R_0 depends on the estimation of the viral infectivity rate, β. In the experimental design, animals were inoculated with a total number of 10^{10} RNA copies and 10^6 pfu. Although only a small proportion of established the infection in the considered compartments (total V_0 equal to 8.10^7, see Table 1), this nonetheless implies that a large number of cells are probably readily infected upon inoculation, making it difficult to precisely estimate the rate of infection by circulating virus. This led to uncertainty in the estimate of R_0 with a 95% confidence interval ranging between 1 and 18 in both compartments.

Table 1
Population parameter estimates of the final model described by Eq. (1) to (5)

Parameters (units)	Fixed effects (RSE%)	SD of random effects (RSE%)
β_T (mL/copie/d)	1.8×10^{-4} (24)	0.3 (45)
β_N (mL/copie/d)	2.5×10^{-5} (54)	
p_T (copies/d)	1.9×10^{4} (37)	1.0 (26)
p_N (copies/d)	3.6×10^{4} (34)	
V_{T0} (copies)	7.4×10^{7} (15)	-
V_{N0} (copies)	8.2×10^{6} (15)	-
δ (1/d)	1.88 (9)	0.2 (36)
c (1/d)	10 (fixed)	-
k (1/d)	3 (fixed)	-
T_T (t = 0) (cells)	2.25×10^{4} (fixed)	-
T_T (t = 0) (cells)	1.25×10^{5} (fixed)	
σ_T	1.06 (6)	-
σ_N	1.19 (6)	-

Second, we fixed the ratio of infectious virus μ based on the analysis of the virus culture at day 3, showing a ratio of 10^{-4} to 10^{-5} between the number of RNA copies and the number of virus that could grow, expressed in $TCID_{50}$. This is based on VeroE6 cell cultures which may have different susceptibility than tracheal cells. Since this ratio represents a lower bound of the number of infectious virus (since not all infectious virus may grow), we fixed $\mu = 0.001$ and we conducted a sensitivity analysis to verify the robustness of our results to this assumption. Because no virus could grow at subsequent time points, we could not verify our hypothesis that infectious virus and total virus had similar kinetics of decline.

Third, the number of target cells was fixed to 0.1% of the total susceptible cells. This hypothesis is supported by the fact that in humans 0.1% of alveolar type II cells expressing the ACE2 receptor, gate for SARS-CoV-2 to enter host cells [17,18]. Such estimate is unknown to our knowledge in cynomolgus macaques. Although the estimate of T_0 should therefore be taken with caution, we nonetheless note that

it is consistent with the burst size of the virus. Indeed, we estimated the burst size of infectious virus $\frac{\mu p}{\delta}$ to be equal to 9.6 and 18.3 in the tracheal and nasopharyngeal compartments, respectively, which is consistent with the estimate of secondary infection, R_0, estimated in the two compartments. Fourth, we relied only on measures in both compartments, which may not reflect the kinetics in the lower respiratory tract. It is in particular possible that the kinetics of both the virus and the immune response may be different in the lung, and that both cytokine responses and the lesions as observed by CT scans may be associated with viral loads in the lungs. In our experiments the first viral load measurements in bronchoalveolar lavages (BAL) was made at 6 dpi, and were all below the limit of detection at the next available data point at day 14, precluding a more detailed analysis of the kinetics in the lungs.

We also evaluated the potential role of immunity in viral resolution by investigating several immune response models. We considered 4 models of the immune response involving IFN-γ concentrations [11,19] but none of them showed any strong improvement of data fitting. This is not surprising since none of the cytokines measured here were related to viral dynamics (Fig. 5). As pointed out above, this may be due to the fact that we only relied on data in the URT but may also reflect the fact that the infection in NHPs was mild. This is consistent with data obtained in patients with an asymptomatic infection, in which the immune response and the cytokine response remained low throughout the infection period [20].

Finally, we evaluated whether the parameters found in macaques could be relevant for human infection. To do this, we used the same parameter values and we only modified two parameters to be reflective of human infection. First we used the same number of target cells as previously estimated in human URT [21,22] ; second, we assumed that the infection was initiated by only one infectious virus (see more discussions on the number of virus in droplets during small speeches [23]). Interestingly, our model could well recapitulate a typical viral kinetic curve. Indeed, we found that the viral load measured on nasopharyngeal swabs peaked at day 4 ($CI_{95\%}$ = [2.2–8.7]) post infection, which is similar to results found in prospective cohorts of asymptomatic or mild infections [24]. Interestingly, the predicted duration of viral shedding was 10.4 days ($CI_{95\%}$ = [8.9–16.6]), remarkably in line with estimates of 9 days [25] and 12 days [9], but lower than other estimates of about 20 days [20,24]. Moreover, we could use the model to predict the course of infectious virus. We predicted that infectious virus was below the limit of detection at day 7, which is also earlier than the estimates of Van Kampen, obtained in severe or critical patients, where the probability to detect infectious virus dropped below 5% at day 15 post symptoms onset [26]. By characterizing the course of infectious virus, we predicted the generation time which indicates the speed at which the infection spreads in the population, to be about 4 days ($CI_{95\%}$ = [2.8–7.6]). This can be put in perspective with the estimate of the serial interval of 5.8 days estimated in cohorts of transmission pairs [24]. All together, these results demonstrate that the viral dynamic parameters obtained in this experimental model are close to those obtained in human mild infection but they may be less relevant for severe infection, characterized by cytokine elevation [27], higher levels of viral load [28] and presumably longer time of viral shedding [8].

Material And Methods

Experimental procedure

Our study includes 31 cynomolgus macaques (16 male, 15 female) infected with 10^6 pfu of a primary isolate of SARS-CoV-2. Each animal received 5 mL of the total inoculum: 4.5 mL were injected by the intra-tracheal route and 0.5 mL by the intra-nasal route. Nasopharyngeal and tracheal swabs were collected longitudinally at days 1, 2, 3, 4, 5, 7, 9, 11, 13, 16 and 20 post-infection (pi). In parallel, broncho-alveolar lavages were collected at day 6, 13 and 20. Viral RNA levels were assessed in each sample using a real-time PCR, with 8540 and 180 copies/mL as quantification and detection limits, respectively.

The original study included 6 groups treated either by a high dosing regimen (Hi) of HCQ (90 mg/kg loading dose and 45 mg/kg maintenance dose) ± AZM (36 mg/kg of at 1 dpi, followed by a daily maintenance dose of 18 mg/kg), a low dosing regimen (Lo) of HCQ (30 mg/kg loading dose and 15 mg/kg maintenance dose) or a vehicle (water) as a placebo. Among the 23 treated animals, 14 were treated at 1 dpi with a Lo (n = 4), Hi (n = 5) dose of HCQ or HCQ + AZTH (n = 5). A late treatment initiation was also investigated in 4 animals receiving a Lo dosing regimen. Finally, 5 animals received HCQ at the Hi dose starting at day 7 prior to infection as a pre-exposure prophylaxis (PrEP). Given that HCQ was not associated to an antiviral effect [14], we pooled the data from either treated and untreated groups. Thus, we consider all animals as controls in our primary analysis but we investigated a potential effect of HCQ in reducing the viral production p (see supplementary information file 1).

Viral dynamic model of SARS-CoV-2

Model describing nasopharyngeal and tracheal swabs

We developed a viral kinetic model that simultaneously characterizes nasopharyngeal and tracheal SARS-CoV-2 infection kinetics (**Fig. 2**). In this model, both nasopharynx and trachea were considered as distinct compartments, each one described by a target cell limited models [15,16]. In the following, only a generic description of the model is presented and subscripts were omitted. Target cells (T) are infected by infectious viruses (V^I) at an infectivity rate β. After infection, infected cells enter an eclipse phase (I_1) where they do not produce virions and enter into productively infected cells (I_2) at a rate k. I_2 cells produce p virions daily and are lost at a *per capita* rate δ. A proportion μ of the virions are infectious (V^I) and the remaining (1-μ) are noninfectious viruses (V^{NI}). Finally, both V^I and V^{NI} are cleared at a rate c.

Fixed parameters

Because not all parameters could be properly estimated based on total RNA data only, some parameters had to be fixed based on the experimental setting or the current literature. First, the term pT_0 is the only identifiable quantity in our model, were T_0 is the initial amount of susceptible cells at the beginning of the infection. Given the estimated surface of the trachea (S_T= 9 cm^2) and nasal cavities (S_N=50 cm^2) in

cynomolgus macaques (data not shown) and the apical surface of one epithelial cell s=4 10^{-7} cm^2/cell [21], one can calculate the number of target cells exposed to the virus in the nasopharynx and the trachea $\frac{S_N}{s} = 1.25 \times 10^8$ and $\frac{S_T}{s} = 2.25 \times 10^7$, respectively. However, only a small fraction of these cells may express the ACE2 receptors needed for SARS-CoV-2 to enter a cell. Hence, assuming a proportion of 0.1% of cells expressing the ACE2 receptor, we set $T_N(t=0) = 1.25 \times 10^5$ and $T_T(t=0) = 2.25 \times 10^4$cells in nasopharynx and trachea respectively. Second, we supposed the proportion of infectious viruses μ remained constant over time and equal to 0.001. Indeed, infectious titers measured by cell culture on tracheal swabs taken at 3 dpi (see details in supplementary information file 3) ranged from 1.2 to 3.2 $\log_{10}$ $TCID_{50}$/mL i.e. 1,000 to 100,000 times lower than total RNA (**Fig. 7**).Third, we supposed that the eclipse phase duration was equal in the nasopharynx and in the trachea, and we set k=3 d^{-1} as the viral loads have been shown to increase 8h after infection [29]. Fourth, the viral clearance c was assumed equal whatever the infectious nature of the virus and its location. Thus, we fixed c to 10 d^{-1} as the clearance is assumed to be fast in other respiratory infections [16]. A sensitivity analyses was conducted with diffentent values of c and k (see supplementary information file 4). Lastly we derived secondary parameters summarizing the infection, namely the basic reproduction number $R_0 = \frac{\beta p T_0 \mu}{c\delta}$ and the burst-size $N = \frac{p}{\delta}$.

Statistical model

The structural model used to describe the observed $\log_{10}$ viral loads $Y_{ijk}$of the i^{th} animal at the j^{th}time point in the k^{th} compartment (nasopharyngeal or tracheal)is

$$Y_{ijk} = f(\theta_i, t_{ijk}) + e_{ijk} \qquad (6)$$

where θ_i is the vector of parameters of subject i and e_{ijk} is the additive residual error. Individual parameters θ_i are supposed to follow a log-normal distribution:

$$\theta_i = \gamma \times exp(\eta_i) \quad (7)$$

where γ indicates the fixed effects and η_i the random effects, which are supposed to follow a normal distribution of mean zero and standard deviation ω. The residual error e_{ijk} is assumed to follow a normal distribution of mean zero and constant standard deviation σ_k.

Standard errors were calculated by drawing parameters in the asymptotic distribution of the parameter estimators. For each parameter, we calculated the 2.5 and 97.5% percentile to derive the 95% confidence interval.

Modelling strategy

In order to reduce the number of parameters, we tested whether the transition rate between nasopharynx and trachea g could be set to 0. Then, we tested the possibility for parameters β, δ, p and V_0 to be equal in both nasopharynx and trachea and tested if their variances could be set to 0. To do this, we used a

backward selection procedure and stopped once the BIC did not decrease anymore. Lastly, based on the Empirical Bayes Estimates (EBE), we screened the random effects for correlations. Only correlations with a Pearson's coefficient >0.8 were implemented in the model.

Plasma cytokine analysis

In all 31 macaques, the concentration of 30 cytokines were measured at 0, 2, 5, 7 and 9 dpi. Among them, CCL11, CCL2, IFN-, Il-15, Il-1Ra and Il-2 were of particular interest as their kinetic changed during the infection (**Fig. 4**). To identify the cytokines to be incorporated in the model, we correlated the are under the cytokine curve (AUC, calculated by the linear trapezoidal method) with the AUC of $\log_{10}$ viral loads predicted by the model and calculated Spearman correlations (**Fig. 5**). Eventually, Spearman correlations with p-value<0.1 were further investigated and implemented in the viral dynamic model. In addition, we tested models involving IFN-, a central element of the immune response against SARS-CoV-2 in humans [27].

Parameter estimation

Parameters were estimated with the SAEM algorithm implemented in MONOLIX® software version 2018R2 allowing to handle the left censored data [30]. Likelihood was estimated using the importance sampling method and the Fisher Information Matrix (FIM) was calculated by stochastic approximation. Graphical and statistical analyses were performed using R version 3.4.3.

Simulation of the infection time course in humans

Assuming that the number of viruses entering a host is low in humans, the infection would start after a virus had infected its first cell. Thus, we scaled the compartments to human size considering a total URT cell count of $4x10^8$ and 30 mL of volume [16,22] and assumed that the infection started after infection of one productive infected cell in the nasopharynx and in the trachea (i.e. $I_{2,N} = I_{2,T} =$ 1 cell). We then computed the median and associated $CI_{95\%}$ of peak viral load and viral shedding, as well as the generation time T_g corresponding to mean duration between a primary case and its associated secondary infections assuming that the infectiousness is proportional to the infectious viral load levels $V^I(t)$.

$$T_g = \frac{\int_0^\infty t \times V^I(t)dt}{\int_0^\infty V^I(t)\,dt}$$

Declarations

Acknowledgments

We thank Peter Czuppon (Collège de France & Sorbonne Université), François Blanquart (Collège de France & INSERM UMR1137) and Alan S. Perelson (Los Alamos National Laboratory) for critical reading and expertise on the analysis. The study received financial support of the national research agency (ANR) through the ANR-Flash calls for COVID-19 (TheraCoV ANR-20-COVI-0018) and also of the Bill & Melinda Gates Foundation under grant agreement INV- 017335.

Author contributions

AB: Performed RT-PCR viral quantification and analyzed the data. AG: Developed the mathematical model, analyzed the data and wrote the article AP: Performed in vitro evaluation of HCQ (Vero E6, HAE). BH: Contributed to study design, data analysis and article writing. BL: Contributed to study design and data analysis. CC: Contributed to study design and data analysis. CS: Supervised and coordinated the HCQ PK analysis, contributed to article writing. FD: Coordinated the viral load and infectious titers quantification FT: contributed to in vitro antivirals evaluation JG: Conceived the project, designed the study, data analysis and article writing. JL: contributed to clinical follow up of animals. MA: Coordinated the viral load and infectious titers quantification. MRC: Contributed to study design and data analysis. NDB: Contributed to the animal work and cytokine measurement, analyzed the data and coordinated IDMIT core activities. NE: Developed the qPCR assay and analyzed the data. NK: Contributed to study design and data analysis. OT: Contributed to data analysis. PM: Contributed to project conception and design of the study, contributed to coordination of the experiments and data analysis, and article writing. RHTF: Coordinated the animal core facility, contributed to study design and data analysis. RLG: Conceived the project, designed the study, analyzed the data and contributed to article writing. RM: Contributed to the design of the study, animal work, data analysis and contributed to article writing. SB: Performed RT-PCR viral quantification and analyzed the data. SVDW: Conceived the project, designed the study, provided the viral challenge stock, coordinated the viral load and infectious titers quantification, contributed to data analysis and article writing.TN: Performed CT acquisitions/CT quantification and contributed to article writing. VC: Contributed to data analysis and article writing. XDL: Contributed to study design and data analysis.

Competing interests

Antonio Gonçalves is a PhD funded by ROCHE Company. Dr. Jérémie GUEDJ has worked as consultant for ROCHE Company.

Animal ethics

Cynomolgus macaques (Macaca fascicularis) used in this study aged 37–40 months and originated from Mauritian AAALAC certified breeding centers. Animals were housed in IDMIT facilities (CEA, Fontenay-aux-roses), under BSL-2 and BSL-3 containment when necessary (Animal facility authorization #D92-032-02, Prefecture des Hauts de Seine, France) in compliance with European Directive 2010/63/EU, the French regulations and the Standards for Human Care and Use of Laboratory Animals of the Office for Laboratory Animal Welfare (OLAW, assurance number #A5826-01, US). Protocols were approved by

the institutional ethical committee “Comité d’Ethique en Expérimentation Animale du Commissariat à l’Energie Atomique et aux Energies Alternatives” (CEtEA #44) under statement number A20-011. The study was authorized by the “Research, Innovation and Education Ministry” under registration number APAFIS#24434- 2020030216532863v1.

References

1. Chen, N. *et al.* Epidemiological and clinical characteristics of 99 cases of 2019 novel coronavirus pneumonia in Wuhan, China: a descriptive study. *The Lancet* **395**, 507–513 (2020).
2. Yang, X. *et al.* Clinical course and outcomes of critically ill patients with SARS-CoV-2 pneumonia in Wuhan, China: a single-centered, retrospective, observational study. *The Lancet Respiratory Medicine* **8**, 475–481 (2020).
3. Wu, F. *et al.* Neutralizing antibody responses to SARS-CoV-2 in a COVID-19 recovered patient cohort and their implications. *medRxiv* (2020) doi:10.1101/2020.03.30.20047365.
4. Hu, B., Huang, S. & Yin, L. The cytokine storm and COVID-19. *J. Med. Virol.* (2020) doi:10.1002/jmv.26232.
5. Guedj, J., Bazzoli, C., Neumann, A. U. & Mentré, F. Design evaluation and optimization for models of hepatitis C viral dynamics. *Statistics in Medicine* **30**, 1045–1056 (2011).
6. Lovern, M. *et al.* Applications of Influenza Viral Kinetic Modeling in Drug Development. *Curr Pharmacol Rep* **3**, 294–300 (2017).
7. Hill, A. L., Rosenbloom, D. I. S., Nowak, M. A. & Siliciano, R. F. Insight into treatment of HIV infection from viral dynamics models. *Immunol Rev* **285**, 9–25 (2018).
8. Zheng, S. *et al.* Viral load dynamics and disease severity in patients infected with SARS-CoV-2 in Zhejiang province, China, January-March 2020: retrospective cohort study. *BMJ* **369**, (2020).
9. Young, B. E. *et al.* Epidemiologic Features and Clinical Course of Patients Infected With SARS-CoV-2 in Singapore. *JAMA* (2020) doi:10.1001/jama.2020.3204.
10. Woelfel, R. *et al.* Clinical presentation and virological assessment of hospitalized cases of coronavirus disease 2019 in a travel-associated transmission cluster. *medRxiv* (2020) doi:10.1101/2020.03.05.20030502.
11. Best, K. *et al.* Zika plasma viral dynamics in nonhuman primates provides insights into early infection and antiviral strategies. *Proceedings of the National Academy of Sciences* **114**, 8847–8852 (2017).
12. Madelain, V. *et al.* Ebola viral dynamics in nonhuman primates provides insights into virus immuno-pathogenesis and antiviral strategies. *Nat Commun* **9**, 4013 (2018).
13. Guedj, J. *et al.* Antiviral efficacy of favipiravir against Ebola virus: A translational study in cynomolgus macaques. *PLOS Medicine* **15**, e1002535 (2018).
14. Maisonnasse, P. *et al.* Hydroxychloroquine in the treatment and prophylaxis of SARS-CoV-2 infection in non- human primates. *Nature* (2020).

15. Pawelek, K. A. *et al.* Modeling within-host dynamics of influenza virus infection including immune responses. *PLoS Comput Biol* **8**, e1002588 (2012).
16. Baccam, P., Beauchemin, C., Macken, C. A., Hayden, F. G. & Perelson, A. S. Kinetics of influenza A virus infection in humans. *J Virol* **80**, 7590–7599 (2006).
17. Bezara, M. E. O. *et al. Heterogeneous expression of the SARS-Coronavirus-2 receptor ACE2 in the human respiratory tract*. http://biorxiv.org/lookup/doi/10.1101/2020.04.22.056127 (2020) doi:10.1101/2020.04.22.056127.
18. Muus, C. *et al.* Integrated analyses of single-cell atlases reveal age, gender, and smoking status associations with cell type-specific expression of mediators of SARS-CoV-2 viral entry and highlights inflammatory programs in putative target cells. *bioRxiv* 2020.04.19.049254 (2020) doi:10.1101/2020.04.19.049254.
19. Gonçalves, A., Mentré, F., Lemenuel-Diot, A. & Guedj, J. Model Averaging in Viral Dynamic Models. *AAPS J* **22**, 48 (2020).
20. Long, Q.-X. *et al.* Clinical and immunological assessment of asymptomatic SARS-CoV-2 infections. *Nat Med* (2020) doi:10.1038/s41591-020-0965-6.
21. Fedoseev, G. & Geharev, S. *Basic defence mechanisms of bronchio-lung system*. vol. vol 1 Medicina (1989).
22. Ménache, M. G. *et al.* Upper Respiratory Tract Surface Areas And Volumes of Laboratory Animals And Hhumans: Cconsierations for Dosimetry Models. *Journal of Toxicology and Environmental Health* **50**, 475–506 (1997).
23. Stadnytskyi, V., Bax, C. E., Bax, A. & Anfinrud, P. The airborne lifetime of small speech droplets and their potential importance in SARS-CoV-2 transmission. *PNAS* **117**, 11875–11877 (2020).
24. He, X. *et al.* Temporal dynamics in viral shedding and transmissibility of COVID-19. *Nature Medicine* **26**, 672–675 (2020).
25. Sakurai, A. *et al.* Natural History of Asymptomatic SARS-CoV-2 Infection. *N Engl J Med* NEJMc2013020 (2020) doi:10.1056/NEJMc2013020.
26. Kampen, J. J. A. van *et al.* Shedding of infectious virus in hospitalized patients with coronavirus disease-2019 (COVID-19): duration and key determinants. *medRxiv* 2020.06.08.20125310 (2020) doi:10.1101/2020.06.08.20125310.
27. Hadjadj, J. *et al.* Impaired type I interferon activity and exacerbated inflammatory responses in severe Covid-19 patients. *medRxiv* 2020.04.19.20068015 (2020) doi:10.1101/2020.04.19.20068015.
28. To, K. K.-W. *et al.* Temporal profiles of viral load in posterior oropharyngeal saliva samples and serum antibody responses during infection by SARS-CoV-2: an observational cohort study. *The Lancet Infectious Diseases* **20**, 565–574 (2020).
29. Agostini, M. L. *et al.* Coronavirus Susceptibility to the Antiviral Remdesivir (GS-5734) Is Mediated by the Viral Polymerase and the Proofreading Exoribonuclease. *mBio* **9**, (2018).

30. Samson, A., Lavielle, M. & Mentré, F. Extension of the SAEM algorithm to left-censored data in nonlinear mixed-effects model: Application to HIV dynamics model. *Computational Statistics & Data Analysis* **51**, 1562–1574 (2006).

Figures

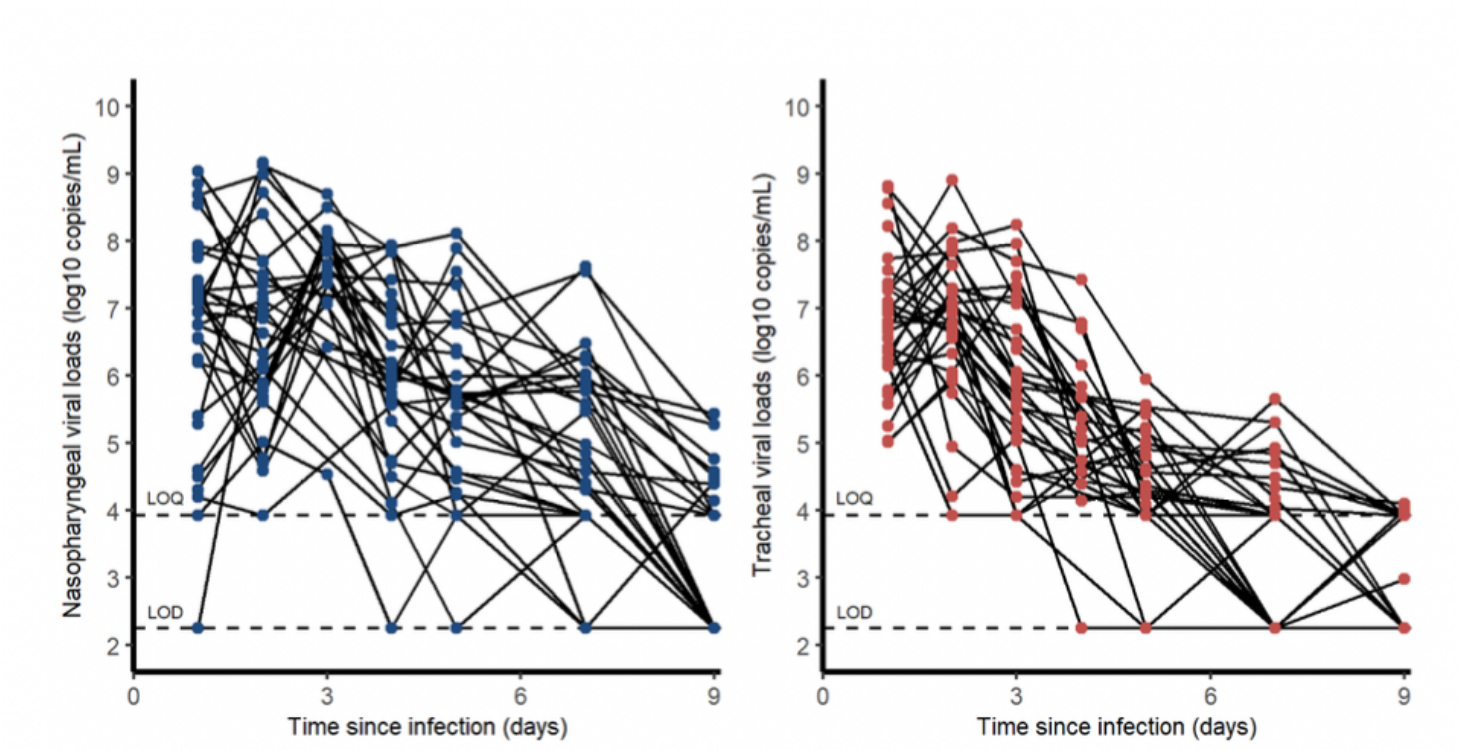

Figure 1

Nasopharyngeal and tracheal SARS-CoV-2 viral loads in infected cynomolgus macaques treated by hydroxychloroquine ± azithromycin. Dashed lines represent the lower limit of detection (LOD) and lower limit of quantification (LOQ).

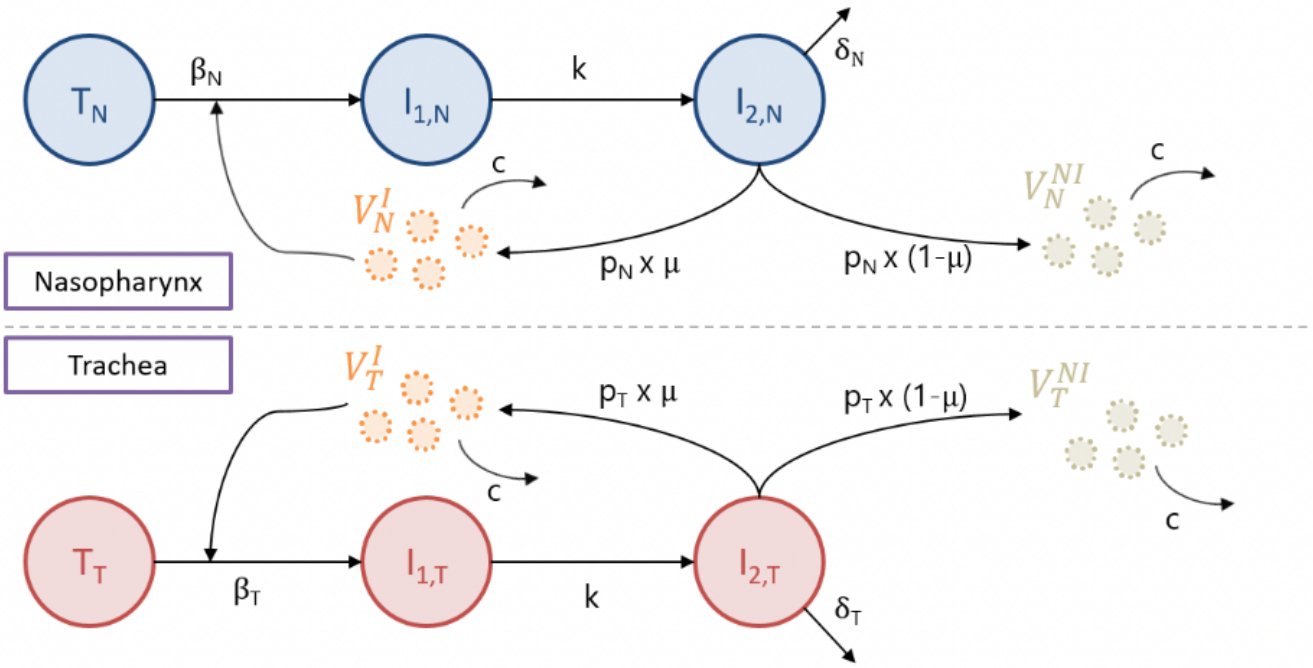

Figure 2

Schematic representation of the model of nasopharyngeal and tracheal viral loads. Parameters c, k and μ were assumed identical in nasopharynx and trachea while we tested wheter β, p and δ could be different in both compartments (see methods)

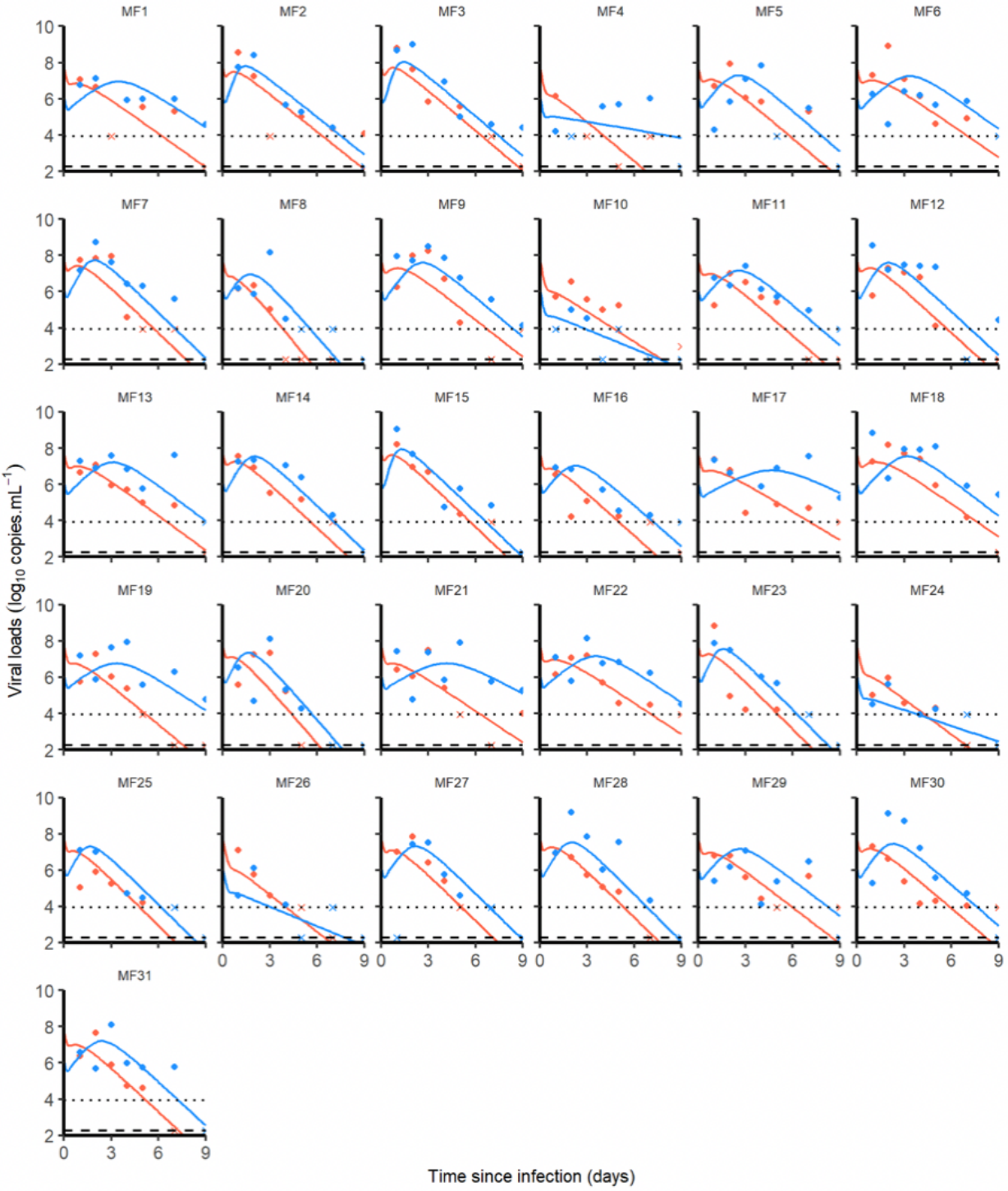

Figure 3

Nasopharyngeal (blue) and tracheal (red) individual predicted dynamics by the model described in equations (1) to (5). Full dots are the quantifiable viral loads and crosses the observation below the limit of quantification. The dotted line represents the limit of quantification and the dashed line the limit of detection.

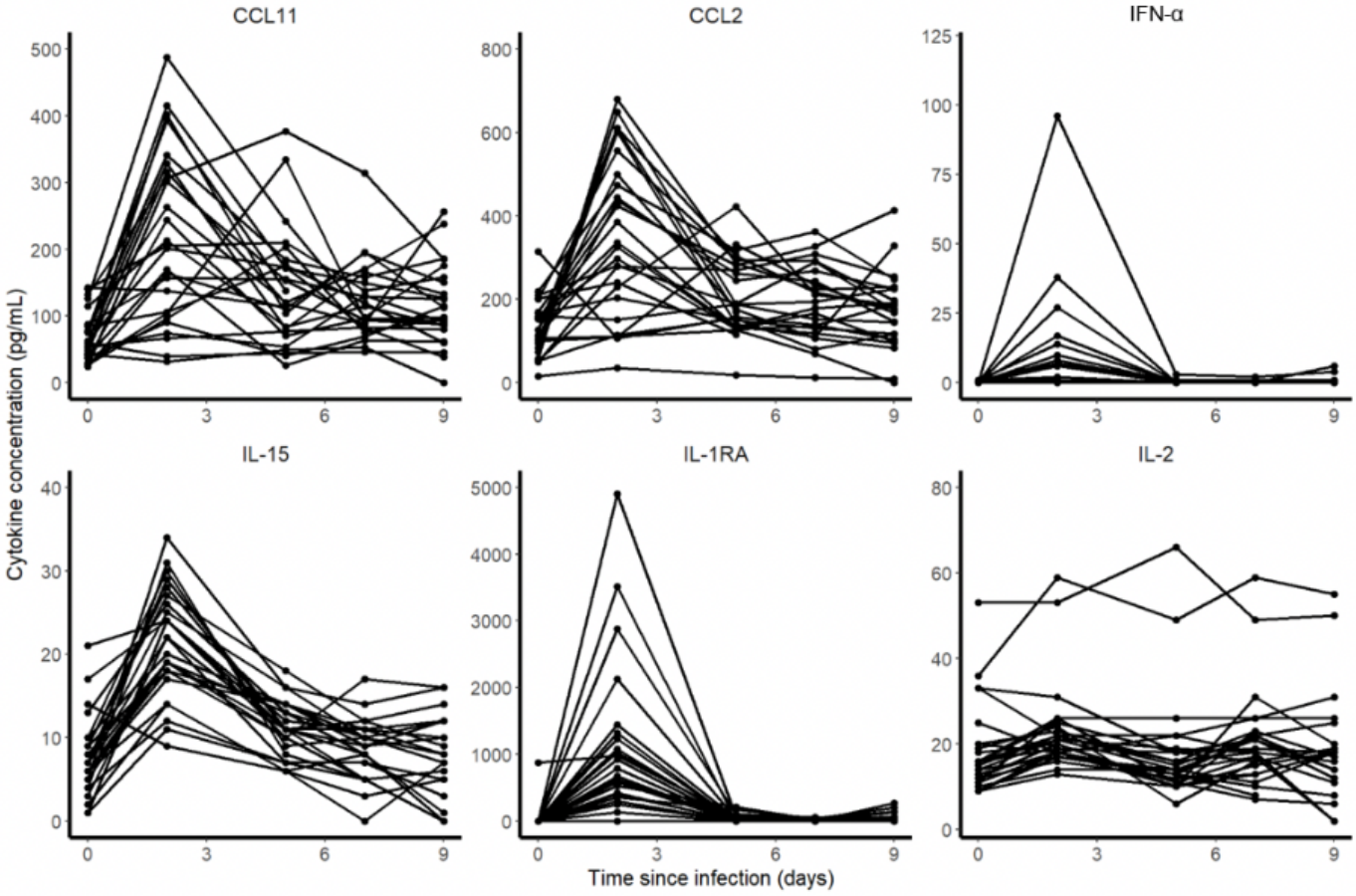

Figure 4

Cytokine concentrations during SARS-CoV-2 infection

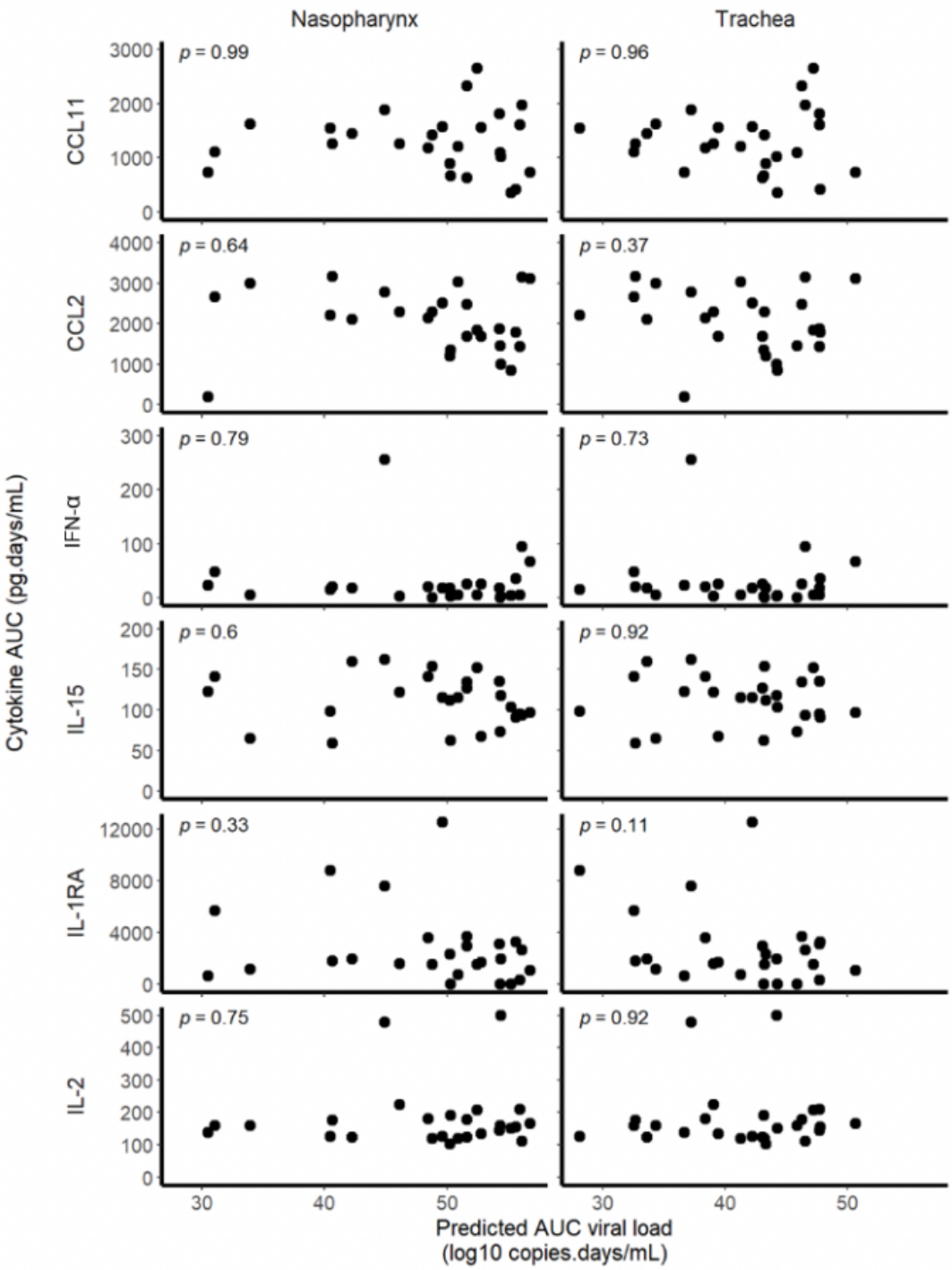

Figure 5

Correlation between the individual predicted AUC log10 viral load and cytokine AUC

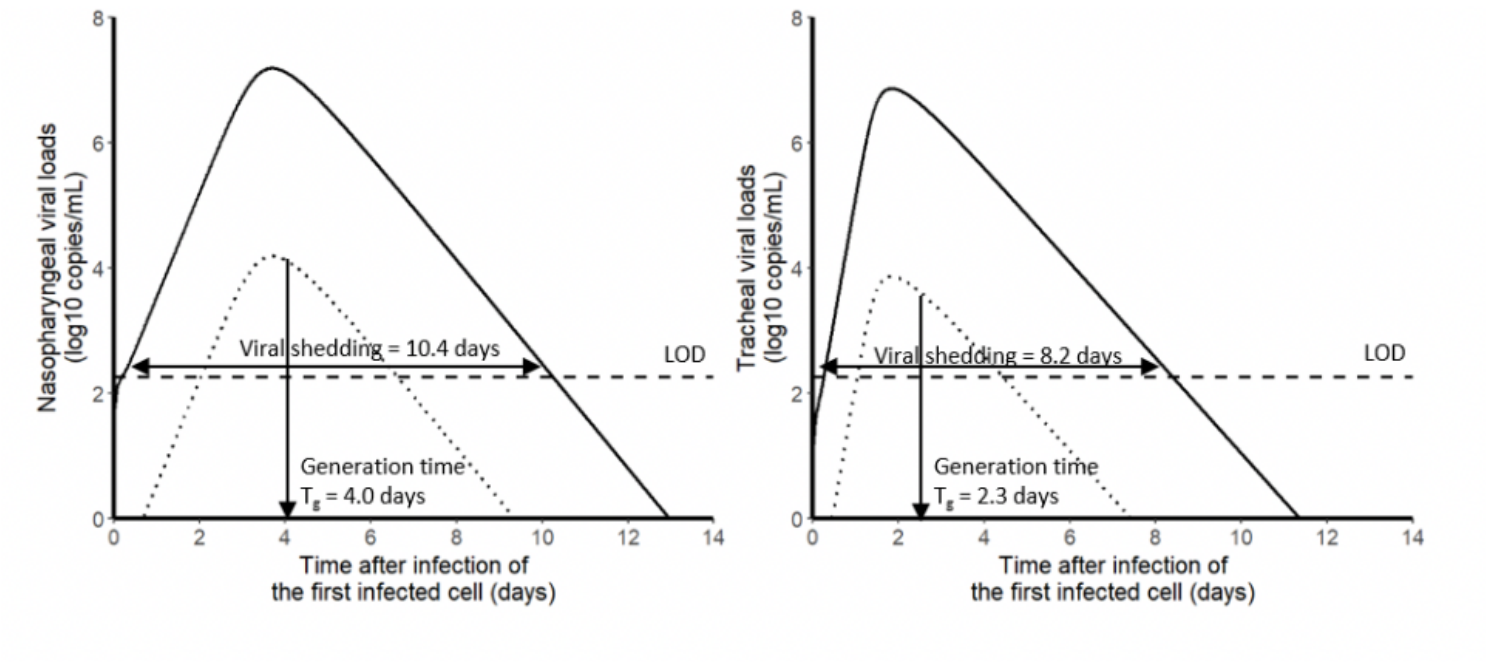

Figure 6

Simulated profile of nasopharyngeal and tracheal log10 viral loads in humans supposing an infection starting with one infected cell. Solid line represents the total viral loads and the dotted line represents the infectious titers.

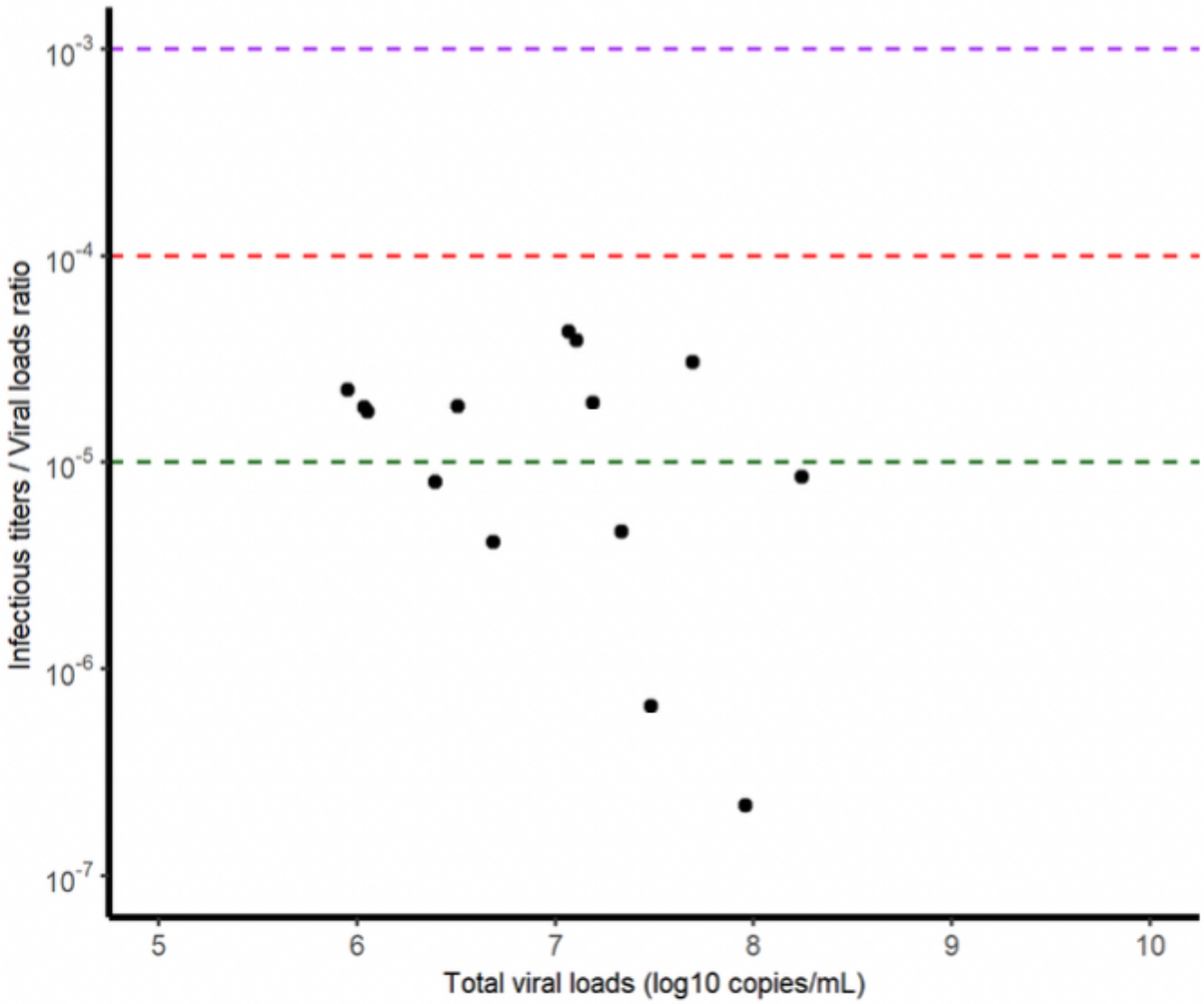

Figure 7

Relationship between infectious titers/total viral load ratio and total viral loads. Each dot corresponds to a tracheal swab at 3 dpi used to measure the infectious titers (see supplementary information file 3) and the total viral loads. Green, red and purple dashed lines correspond to ratios of 10-5, 10-4 and 10-3 respectively.

Supplementary Files

This is a list of supplementary files associated with this preprint. Click to download.

- SI1HCQeffect.docx
- SI2immuneresponse.docx
- SI3infectioustiters.docx
- SI4sensitivityanalysis.docx